Colloids and Surfaces B: Biointerfaces 217 (2022) 112679

Contents lists available at ScienceDirect

Colloids and Surfaces B: Biointerfaces

journal homepage: www.elsevier.com/locate/colsurfb

Bonding antimicrobial rhamnolipids onto medical grade PDMS: A strategy to overcome multispecies vascular catheter-related infections

Maïssa Dardouri [a], Israa M. Aljnadi [a], Jonas Deuermeier [b], Catarina Santos [c,d], Fabiola Costa [e,f], Victor Martin [g,h], Maria H. Fernandes [g,h], Lídia Gonçalves [a], Ana Bettencourt [a], Pedro Sousa Gomes [g,h], Isabel A.C. Ribeiro [a,*,1]

[a] Research Institute for Medicines (iMed.ULisboa), Faculty of Pharmacy, Universidade de Lisboa, Avenida Prof. Gama Pinto, 1649-003 Lisboa Portugal
[b] CENIMAT=i3N, Department of Materials Science, School of Science and Technology, NOVA University Lisbon and CEMOP/UNINOVA, 2829-516 Caparica, Portugal
[c] CQE Instituto Superior Técnico, Universidade de Lisboa, Av. Rovisco Pais, 1049-001 Lisboa, Portugal
[d] EST Setúbal, CDP2T, Instituto Politécnico de Setúbal, Campus IPS, 2910 Setúbal, Portugal
[e] i3S – Instituto de Investigação e Inovação em Saúde, Universidade do Porto, Rua Alfredo Allen, 208, 4200-135 Porto, Portugal
[f] INEB – Instituto de Engenharia Biomédica, Universidade do Porto, Rua Alfredo Allen, 208, 4200-135 Porto, Portugal
[g] Laboratory for Bone Metabolism and Regeneration – Faculty of Dental Medicine, U. Porto Rua Dr. Manuel Pereira da Silva, 4200-393 Porto, Portugal
[h] LAQV/REQUIMTE, U. Porto, Porto 4160-007, Portugal

ARTICLE INFO

Keywords:
Antimicrobials
Medical devices
PDMS
Antibiofilm
Rhamnolipids
Biosurfactants
Staphylococcus aureus
Candida albicans
Staphylococcus epidermidis

ABSTRACT

In clinic there is a demand to solve the drawback of medical devices multispecies related infections. Consequently, different biomaterial surfaces, such as vascular catheters, urgently need improvement regarding their antifouling/antimicrobial properties. In this work, we covalently functionalized medical grade polydimethylsiloxane (PDMS) with antimicrobial rhamnolipids to investigate the biomaterial surface activity towards mono and dual species biofilms. Preparation of surfaces with "piranha" oxidation, followed by APTES bonding and carbodiimide reaction with rhamnolipids effectively bonded these compounds to PDMS surface as confirmed by FTIR-ATR and XPS analysis. Generated surfaces were active towards *S. aureus* biofilm formation showing a 4.2 log reduction while with *S. epidermidis* and *C. albicans* biofilms a reduction of 1.2 and 1.0 log reduction, respectively, was observed. Regarding dual-species testing the higher biofilm log reduction observed was 1.9. Additionally, biocompatibility was assessed by cytocompatibility towards human fibroblastic cells, low platelet activation and absence of vascular irritation.

Our work not only sheds light on using covalently bonded rhamnolipids towards dual species biofilms but also highlights the biocompatibility of the obtained PDMS surfaces.

1. Introduction

For decades, many polymeric materials have been elected for medical use [1–3]. Among those polydimethylsiloxane (PDMS) is a promising elastomer for numerous applications including for catheters fabrication due to its high flexibility, low cost, biocompatibility, chemical inertness and transparency [4,5]. However, hydrophobicity has been defined as the major obstacle of the use of this biomaterial as it can lead to proteins and microorganism adsorption as well as biofilm development [6]. Similarly, to other materials, microbial PDMS surface contamination is of serious concern, and very challenging to treat specially when caused by a combination of microorganisms (e.g. *S. aureus*, *S. epidermidis* and *C. albicans* [7–9]) often leading to biofilm-associated mixed infections [7].

Thus, there is a demand to solve this pressing problem by changing PDMS surface properties and increasing its antimicrobial properties. This has guided many research groups towards the development of new strategies to render the PDMS surface hydrophilic and resistant to protein adsorption and microbial contamination. These strategies include the coating of PDMS surface with antifouling polymers (e.g., poly(styrenesulfonate), polyethylene glycol, polyvinyl alcohol [10,11]) or antimicrobials such as quaternary ammonium compounds [12,13],

* Correspondence to: Faculty of Pharmacy, Universidade de Lisboa, Avenida Prof. Gama Pinto, 1649-003 Lisboa, Portugal.
E-mail address: iribeiro@ff.ulisboa.pt (I.A.C. Ribeiro).
[1] ORCID: 0000-0002-7110-6393

https://doi.org/10.1016/j.colsurfb.2022.112679
Received 8 April 2022; Received in revised form 30 May 2022; Accepted 28 June 2022
Available online 3 July 2022

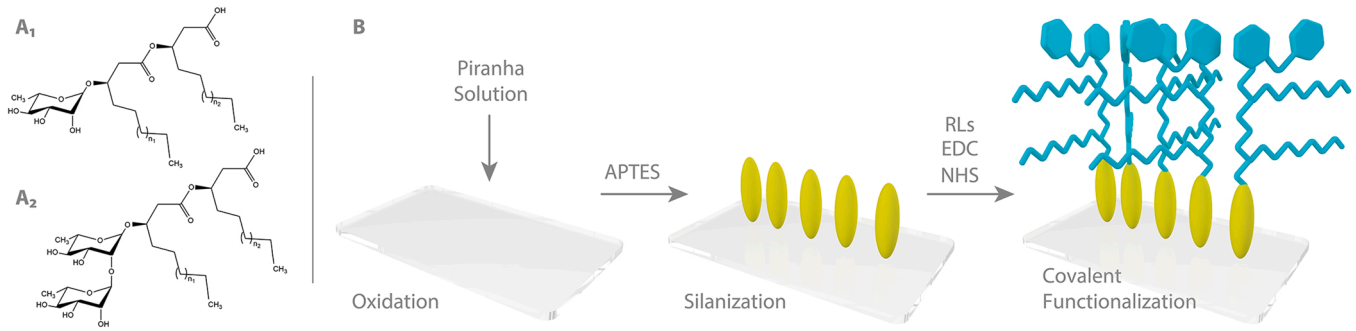

Fig. 1. A. Mono (A_1) and di-RLs (A_2) present in RLs mixture. **B.** Representation of PDMS surface functionalization with antimicrobial RLs through carbodiimide reaction.

antibiotics (e.g. minocycline, rifampicin [14–16]), antimicrobial peptides [3,17] or different nanoparticles (e.g. silver). The active molecules have been attached to the surface either by weak and short-lasting interactions (e.g. physisorption or chemisorption) [18] or long-lasting approaches like covalent bonding (e.g. plasma induced covalent-immobilization; chemical vapor deposition, polymer grafting) [13,19,20]. While these approaches have successfully evidenced the improvement of surface hydrophilicity, their broader use for PDMS anti-biofilm properties is often limited by chemical stability, the need for special equipment (in the case of plasma-induced), the antibiotic resistance crisis [21,22] and lack of reports on mixed infections testing. These issues emphasize the need for evaluating new approaches.

In this paper we focused on an alternative, practical and simple strategy to create a more PDMS hydrophilic surface, with lower protein adsorption profile and antimicrobial properties including against mixed infections based on chemical etching using "piranha reaction", silanization and rhamnolipids incorporation into the surface. Chemical etching aimed a long-lasting modification starting with the oxidation of the surface using "piranha solution" pointed as a compatible, low-cost and robust procedure [23]. The oxidation of the surface enables the process of silanization, that is the covering of the surface with an organofunctional alkoxysilane molecule (3-aminopropyltriethoxysilane, APTES) [24,25], owning active functional groups to the PDMS surface such as amine. The amine anchoring groups promoted the binding of rhamnolipids (RLs), natural glycolipid biosurfactant compounds with antibacterial and antifungal properties [25–28]. Additionally, in contrast to antibiotics, RLs have little impact on the environment and do not favor microorganism resistance [22,26].

The hypothesis of this study is that rhamnolipids covalently bonded to polydimethylsiloxane (PDMS) surface have activity towards mono and dual species biofilms. Additionally, functionalized-PDMS surfaces properties were evaluated and wettability, FTIR-ATR and XPS analysis were performed. Further, the potential interest of the proposed strategy was confirmed by protein adsorption evaluation, antibiofilm and biocompatibility studies.

2. Materials and methods

2.1. Chemicals, reagents and materials

The following chemicals and solvents were used as received: sodium chloride from Panreac (Barcelona, Spain); chloroform and ethanol (100%) from Carlo Erba (Val-de-Reuil, France); acetonitrile and hydrochloric acid 37% from Scharlau (Sentmenat, Spain); sulfuric acid 98%, methanol, glacial acetic acid, MES buffer, sodium hydroxide, potassium dihydrogen phosphate and 4-methoxy benzaldehyde(p-anisaldehyde from Merck (Darmstadt, Germany); N-hydroxysuccinimide (NHS), N-(3-Dimethylaminopropyl)-N′-ethyl carbodiimide hydrochloride (EDC), (3-aminopropyl) triethoxysilane (APTES), and D-(+)-glucose monohydrate from Sigma-Aldrich (Saint Louis, USA); hydrogen peroxide (H_2O_2 30%) from VWR chemicals (Leuven, Belgium); Orange G from BDH Chemicals Ltd (Poole England, UK); agar, peptone and yeast extract from Biokar Diagnostics (Beauvais, France).

2.2. Rhamnolipids characterization

P. aeruginosa rhamnolipids were purchased from Sigma (AGAE Technologies, Corvallis Oregon, USA) with a purity of 90%. Rhamnolipids mixture characterization was performed by UHPLC-MS/MS according to a previously described method [29].

2.3. PDMS surface functionalization

2.3.1. Chemical Etching and RLs functionalization

FDA-approved medical grade PDMS (SOVE, Portugal) with 0.5 mm thickness, was cut into 1 × 1 cm squared pieces and functionalization was performed according to Fig. 1. To activate the PDMS surface with hydroxyl groups, a "piranha solution" composed of sulfuric acid and hydrogen peroxide (7:3, v/v) was used (this solution reacts violently with organic solvents and should be handled with care). After cooling for 30 min, the PDMS was immersed in the "piranha solution" for 60 s and then washed 5 times sequentially in ethanol and in deionized water. PDMS was then immersed in (3-aminopropyl) triethoxysilane (APTES) 10% solution (prepared in an ethanol 4% (v/v) solution, adjusted to pH= 4.5 with glacial acetic acid) for 30 min at 50 °C. Then, samples were washed 3 times with Type I (Milli-Q) water. On the other hand, RLs (5 mg, 0.008 mmol) were converted into N-hydroxysuccinimide esters by sequential reaction with N-(3-Dimethylaminopropyl)-N′-ethyl-carbodiimide hydrochloride (EDC, 4.5 mg, 0.024 mmol) for 15 min and then N-hydroxysuccinimide (NHS, 1.35 mg, 0.012 mmol) for 60 min in 1 mL of 0.1 M MES buffer (pH 6.0). This solution was added to the freshly aminated PDMS substrate and left to react for 20 h at RT under agitation (240 rpm, IKA® MS 3 digital). Finally, samples were washed 3 times with Type I (Milli-Q) water and dried under vacuum until further use.

2.3.2. Optimization conditions

Before reaching the final functionalization conditions some parameters were optimized namely: i) chemical etching treatment time: 45, 60 and 120 s; ii) APTES covalent bonding optimization using direct drying under N_2 atmosphere or thermal post-treatment at 65 °C for 10 min; and iii) the proportions of RLs: EDC: NHS concentrations mg mL^{-1}: R_1 (1.66:1.51: 0.90), R_2 (1.66: 1.51: 0.45) and R_3 (5.00: 4.53: 1.36).

2.3.2.1. Oxidation treatment time. Different oxidation times were first tested. PDMS specimens were soaked in the "piranha solution" for 45, 60, and 120 s, washed with Milli Q water and dried under vacuum. Surfaces were then checked for visual alterations namely opacity, smoothness and flatness. Contact angle measurements were also performed to access surface wettability modification.

2.3.2.2. APTES binding assessment. After the oxidation step for 45 s and 60 s, samples underwent an APTES functionalization and PDMS-APTES substrates were either dried under N_2 atmosphere or endure a thermal post-treatment at 65 ° C for 10 min. In order to quantify the exposed primary amine groups (APTES bonding) existing on the PDMS-APTES surfaces the Orange II method previously mentioned by Noel et al. [30] was used by replacing the orange Orange II solution by an Orange G (OG, 14 mg mL^{-1}) solution. A calibration curve of OG ranging from 1.40×10^{-4} to 0.14 mg. mL^{-1} was conducted in order to quantify the OG adsorbed on the samples' surfaces.

2.3.2.3. Proportion of RLs, EDC, NHS. Three RLs' solution with different reagents' proportions (MR_1, MR_2, MR_3) were used. The different experimental conditions corresponded respectively to different proportions of RLs, EDC, NHS concentrations mg mL^{-1} named as different reactions (R): R_1 (1.66: 1.51: 0.90), R_2 (1.66: 1.51: 0.45) and R_3 (5.00: 4.53: 1.36). Thus, the optimized PDMS-APTES substrates were directly immersed in the R_1, R_2 and R_3 RLs' solutions. After 20 h of reaction. Samples were washed three time with Milli-Q water and dried under vacuum. FTIR, contact angle and biofilm assays were conducted in order to evaluate the different conditions.

2.4. Surface characterization

2.4.1. Wettability

The wettability of the functionalized/unfunctionalized PDMS surfaces was performed using the sessile drop technique. At ambient humidity and temperature, digital images of the MilliQ water droplets (2 μL) placed on the substrates' surfaces was captured by a digital microscope (Rohs USB Digital Microscope) and (AMCAP) software. The resultant angles at the droplets and substrates interface were measured using the sessile drop technique with the Image J software (Image J 1.52p, National Institutes of Health, Bethesda, MD). Five individual droplets were analyzed for each sample at 0 and 10 min after deposition. Average was obtained from at least 8 independent measurements.

2.4.2. Fourier-transform infrared spectroscopy (FTIR)

Identification of the functional groups situated on the samples' surfaces was performed using Attenuated Total Reflectance Fourier Transform Infrared spectroscopy (ATR-FTIR), type Thermo Scientific, Class 1 Laser Product Nicolet 6700. All samples were placed on the ATR diamond crystal and the spectra measurements ranged between [4000–800 cm^{-1}] resulting from an average of 128 scans collected with a resolution of 8 cm^{-1}.

2.4.3. XPS

It is known that in XPS analysis with non-conductive materials, a charge compensation technique must be applied, so that the peaks detected in the spectrum cannot be questioned. Carbon is often used for calibration because the carbon peak is found in all samples exposed to the environment. In our study it was adjust the C1s binding energy of PDMS to 284.8 eV as described in the literature [31]. The chemical composition changes on the surface of the functionalized/unfunctionalized samples were investigated by X-ray photoelectron spectroscopy (XPS) using a Kratos AXIS Supra equipped with a monochromatic Al Kα radiation. The pass energy of survey scans was 160 eV and 10 eV for detail scans. Data analysis was done with CasaXPS 2.3.19PR1.0.

2.4.4. Protein adsorption

The Bradford reagent (Biorad, California USA) protocol with bovine serum albumin (BSA, Sigma, Saint Louis, USA) was used for protein adsorption evaluation [32]. Each sample (functionalized and non-functionalized) was placed in a well of a 24-well microtiter plate (MTP) and added of 500 μL of BSA (1 mg mL^{-1}) in NaCl 0.9% aqueous solution. After agitation at 240 rpm (IKA® MS 3 digital) and incubation at 37 °C (Revco Ultima) for 1 h, test solutions were diluted (1:2) and 10 μL of each was added to 200 μL of Bradford reagent diluted in sterilized MiliQ water (1:4) in a 96-well MTP. The microtiter plate was then incubated at room temperature for 10 min, under agitation (120 rpm, IKA® MS 3 digital) and the absorbance was measured at 595 nm in a Microplate Multimode Reader (Anthos, Zenyth 3100). A calibration curve with different BSA solutions (concentrations ranging from 0.05 to 0.6 mg mL^{-1}) was performed in order to quantify the BSA adsorbed onto the samples' surfaces.

2.5. Antibiofilm activity

2.5.1. Microorganisms

Staphylococcus aureus ATCC *25923™*, *S. epidermidis* ATCC *28319™* and *Candida albicans* ATCC 10231™ were obtained from the American Type Culture Collection (ATCC). Aliquots from frozen stocks at − 80°C were used to culture bacteria on tryptic soy agar (TSA, Biokar Diagnostics, Beauvais, France) plates for 24 h and the yeast on Glucose-Peptone-Yeast Extract-Agar (GPYA) plates composed by glucose (2%), peptone (0.5%) yeast extract (0.5%) and agar (1.5%), for 48 h at 37°C.

2.5.2. Planktonic cells susceptibility

Antimicrobial susceptibility of selected strains to RLs mixture was obtained by the Broth Microdilution Method described in CLSI (2017) and Pontes et al. [33,34]. All assayed samples were two-fold diluted in Müeller–Hinton broth (Biokar Diagnostics, France) or RPMI-MOPS (Gibco) for bacteria and yeast respectively, with a final RLs concentration ranging from 1.7 μg mL^{-1} to 800 μg mL^{-1}. The 0.5 McFarland turbidity inoculum prepared in appropriate broth was further diluted to obtain ~5×10^5 CFU mL^{-1} or ~1×10^3 CFU mL^{-1} of bacteria or yeast per well, respectively. Minimum inhibitory concentration (MIC) results were obtained by measurement of absorbance at 595 nm in a Microplate Multimode Detector (Anthos, Zenyth 3100) after 24 h of incubation at 37 °C. All assays were performed with negative controls (not inoculated media) and positive controls (inoculated media). Assays were carried out in three independent experiments.

2.5.3. Biofilm inhibition evaluation

Antibiofilm assays *towards S. aureus, S. epidermidis* and *C. albicans* were carried out as previously reported by Pontes et al. [33]. Briefly, the inoculum was prepared from 24 h cultures by direct colony suspension in Brain Heart Infusion (BHI, Biokar Diagnostics) medium supplemented with glucose 1% (w/v) for bacteria or Tryptic Soy Broth (TSB, Biokar Diagnostics) medium supplemented with glucose 1% (w/v) for yeast. The inoculum was adjusted to 0.5 McFarland units and further diluted by 1:100 using the same medium in each well of the 24 well MTPs housing on the bottom functionalized and non-functionalized samples (controls). The plates were incubated at 37°C for 24 h (Revco scientific, U.S.A). Afterwards, PDMS samples were washed twice with 1 mL of sterile Phosphate Buffered Saline (PBS) to remove the loosely and non-adhered bacteria and biofilm inhibition was assessed by colony forming units (CFU) counts and Scanning Electron Microscopy (SEM) imaging.

2.5.3.1. Biofilm CFUs count. After washing with PBS solution, PDMS samples were transferred into 2 mL tubes containing 1 mL of sterile aqueous NaCl 0.9% and submitted to sonication and vigorous shaking for 4 min each to detach adhered bacteria on surfaces. Suitable dilutions were performed and for CFU quantification an aliquot was spread in TSA (for bacteria) and GPYA (for yeast) plates. Colonies were counted after incubation for 24 and 48 h for bacteria and yeast respectively at 37 °C and results were reported as log (CFU cm^{-2}). Assays were carried out at least in three independent experiments.

2.5.3.2. Biofilm observation through Scanning Electron Microscopy.

Biofilm fixation was performed according to Mendes et al. [24] and Matos et al. [35] as well as SEM imaging analysis. A field emission gun scanning electron microscope FEG-SEM, model JSM7001F (JEOL, Japan) operated at 10 kV was used.

2.5.4. Antibiofilm activity towards multispecies

Evaluation of functionalized samples antibiofilm activity on co-culture assays were performed by co-culturing *S. aureus* with *S. epidermidis*, *S. aureus* with *C. albicans and S. epidermidis* with *C. albicans*. Inocula were prepared as previously described (2.5.2) in BHI medium supplemented with glucose 1% (w/v) for bacteria co-cultures and TSB supplemented with glucose 1% (w/v) for bacteria and yeast co-cultures [36,37]. Antibiofilm activity was assessed by CFU counts and SEM imaging as previously described. For colony counting TSA plates were used for *S. aureus* with *S. epidermidis* while TSA and GPYA plates were used when co-culturing bacteria and yeast.

2.6. Biocompatibility assays

2.6.1. Cytocompatibility assays

Human dermal fibroblasts (AG22719) were obtained from Coriell Institute for Medical Research. Cultures from the 8th passage were grown in α-Minimal Essential Medium (α-MEM), containing 10% fetal bovine serum (FBS), 100 IU/mL penicillin, 100 μg/mL streptomycin and 2.5 μg/mL amphotericin B (all Gibco), incubated at 37 °C and 5% CO_2 in air.

When reached approx. 70% confluency, cells were detached by trypsinization and sub-cultured at 1×10^4 cells/cm^2 for either the direct or indirect assays. Regarding the former, cells were seeded directly over the samples' surfaces, or regarding the latter, on the bottom of the wells with a permeable insert (Transwell 6.5 mm insert, 0.4 μm permeable membrane, Costar) containing the samples, in order to grow the cultures within the material's leachable. Cultures were maintained for 5 days. Material without seeded cells and cells cultured without materials were incubated at the same experimental conditions and were used as blank control and positive control, respectively.

2.6.2. Metabolic activity and cell viability

The tetrazolium dye (MTT) was used to evaluate the metabolic activity and viability of human dermal fibroblasts when cultured directly on the materials. At 1 and 5 days timepoints, MTT solution (Sigma-Aldrich) at 5 mg mL^{-1} was added to each well and incubated at 37 °C for 3 h. Following, attained formazan crystals were dissolved in dimethyl sulfoxide and the absorbance of the MTT product was measured at 550 nm, using a microplate reader (Synergy HT; BioTek).

In addition, the Resazurin assay was employed to evaluate the metabolic activity and viability of cultures in contact with the material's leachables. At day 1 and 5 of culture, the medium of each well was replaced by a mixture of fresh culture medium with 10% Resazurin solution (100 μg/mL, Sigma-Aldrich) for 3 h, at 37 °C. The medium was collected and the fluorescence was measured by a microplate reader (Synergy HT; BioTek - excitation: 530 nm, emission: 590 nm). Five independent experiments were performed.

2.6.3. Cell morphology

Cell morphology was observed using a Celena S digital imaging system (Logos Biosystems) by culture's fluorescence staining, in which filamentous actin (F-actin) and nucleus were marked using phalloidin-conjugated Alexa Fluor 488 (Molecular Probes) and Hoechst 33342 (Enzo), respectively. Briefly, cultured cells at day 1 were fixed with paraformaldehyde 3.7%, permeabilized with Triton-X (Sigma-Aldrich) 0.1% and incubated with bovine serum albumin (Sigma–Aldrich) at room temperature, prior to the immunostaining. Images were processed using the ImageJ software v.1.52a [38].

2.6.4. In vitro hemocompatibility evaluation – platelet adhesion

Regarding the platelet adhesion assay, materials were incubated with citrate anticoagulated blood. Briefly, blood was centrifuged at 2500 RPM for 10 min in order to obtain a platelet rich plasma (PRP) and then, the suspension was diluted in PBS until the concentration of 10^8 platelets/mL was reached. $CaCl_2$ (2.5 mM) and $MgCl_2$ (1.0 mM) were added. Materials and controls (treated plastic and glass, as negative and positive controls, respectively) were hydrated by PBS immersion before the assay. Then, 200 μL of the obtained PRP was added to the samples at 37 °C. After an hour, materials were washed for the removal of non-adhered platelets, fixed in 1.5% glutaraldehyde and a dehydration was performed with progressive concentrations of ethanol and finished with hexamethyldisilazane treatment. Finally, the morphological characterization was conducted by scanning electron microscopy (Quanta 400 FEG ESEM/EDAX Genesis X4M). Representative images of each group were acquired and analyzed.

2.6.5. Evaluation of the irritation potential

HET-CAM (hen's egg-chorioallantoic membrane) test was performed to evaluate the vascular irritation potential of the developed materials. Fresh fertile White Leghorn hen's eggs were incubated at 37 °C and 50% humidity within a rotating egg incubator (Octagon Advance, Brinsea), for 9 days. Subsequently, the incubation was interrupted and the air sac position of the eggs was marked. The eggshell was opened and the CAM was exposed after the removal of the outer membrane. Materials were placed over the CAM, as well as the established controls, in accordance to the Interagency Coordinating Committee on the Validation of Alternative Methods (ICCVAM) guidelines - NaCl 0.9% solution as negative control and NaOH 0.1 N solution as positive control, enclosed by a silicone ring. The irritation reaction was observed over a period of 5 min, searching for vessel lysis, hemorrhage and coagulation. Images were captured during the assay using a Zeiss Stemis 305 stereo microscope, coupled to an Axiocam 5 Color Camera. Five independent experiments were performed.

2.7. Statistical analysis

For protein adsorption assessment, the statistical analysis between the controls and the functionalized samples was performed by applying the unpaired t test method. The statistical significance was set at 95% confidence interval. GraphPad Prism 5 software v.5.03 (GraphPad Software, San Diego, California, USA) was used in order to perform the statistical analysis.

In biocompatibility assessment normality of the data was determined by the Shapiro-Wilk test. In which regards to normally-distributed datasets, one-way analysis of variance (ANOVA) was performed, followed by Tukey post hoc test. Regarding non-normally distributed datasets, Kruskal-Wallis test followed by multiple comparisons using Dunn's test, was performed. p values ≤ 0.05 were considered significant. Statistical analysis was performed in the IBM SPSS statistics 26.0 software.

3. Results and discussion

3.1. Characterization and purification of RLs mixture

RLs' mixture characterization and purification were carried out according to Dardouri et al. [29]. Different RLs' structures were identified by UHPLC-MS/MS including mono and di-rhamnolipids with different combinations of saturated and unsaturated fatty acids. In RLs mixture, di-RLs account for the majority of RLs showing a percentage of 67% when comparing to 33% of mono-RLs. The RhaRhaC10:0C10:0 was identified as the most abundant congener in the mixture (35%). Additionally, among other compounds present it was possible to identify the following congeners: RhaRhaC8:0C10:0, RhaC8:0C10:0, RhaRhaC8:0C12:0, RhaRhaC10:0C10:1, RhaRhaC10:C12:1,

A

	Control	APTES	RLs
Contact angle (°)	95.37 ± 4.28	90.10 ± 5.87	17.26 ± 2.43

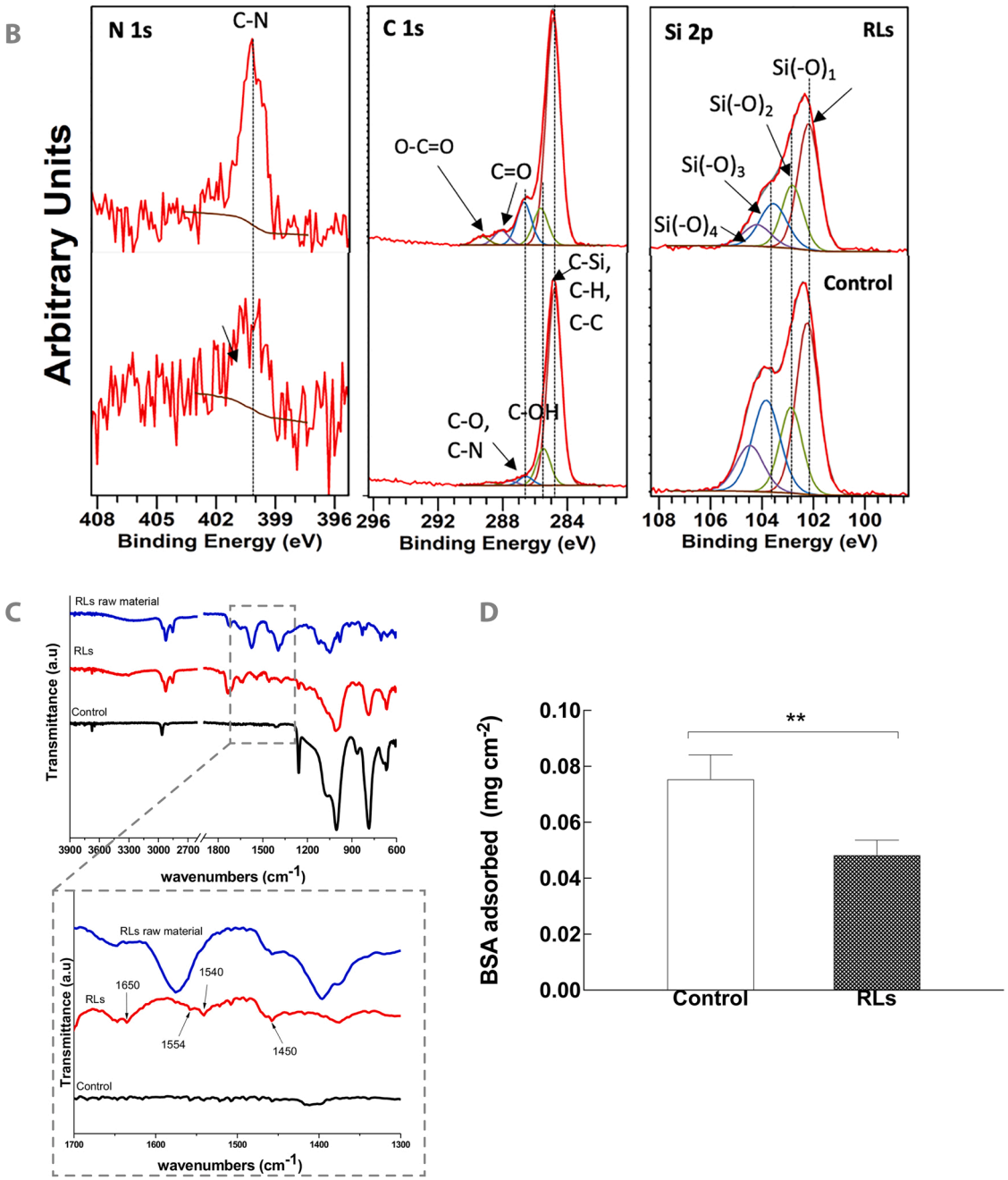

Fig. 2. **A.** Contact angle measurement of PDMS, PDMS-APTES (APTES), PDMS-RLs (RLs) (t = 10 min). **B.** High-resolution XPS N 1 s, C 1 s and Si 2p spectra of the PDMS and PDMS-RLs surface. **C.** Attenuated total reflection-Fourier transform infrared spectroscopy (ATR-FTIR) of the PDMS, PDMS-RLs, and RLs raw materials **D.** Protein adsorption to PDMS and PDMS-RLs surface (** $p < 0.01$).

RhaRhaC10:0C12:0, RhaC10:0C12:1, RhaC10:0C10:1, RhaRhaC10:0C14:1, RhaC10:0C12:0. This is in accordance with the previous work of Chebbi et al. [39] showing the predominance of congeners RhaRhaC10:0C10:0 among mono and di-RLs produced by *P. aeruginosa* W10 and the effectiveness of RLs mixture against the biofilm formation, disruption, and anti-adhesive activity [39].

3.2. Surface characterization and antibiofilm activity of PDMs-RLs

The first step assays related to the optimization of the functionalization parameters (results presented in Supplementary Material SM1) made possible to conclude about the optimal conditions to be used in the subsequent experiments. Specifically, using "piranha etching" for one minute, APTES functionalization without post-thermal treatment followed by R_3 proportion solution used for RLs' functionalization.

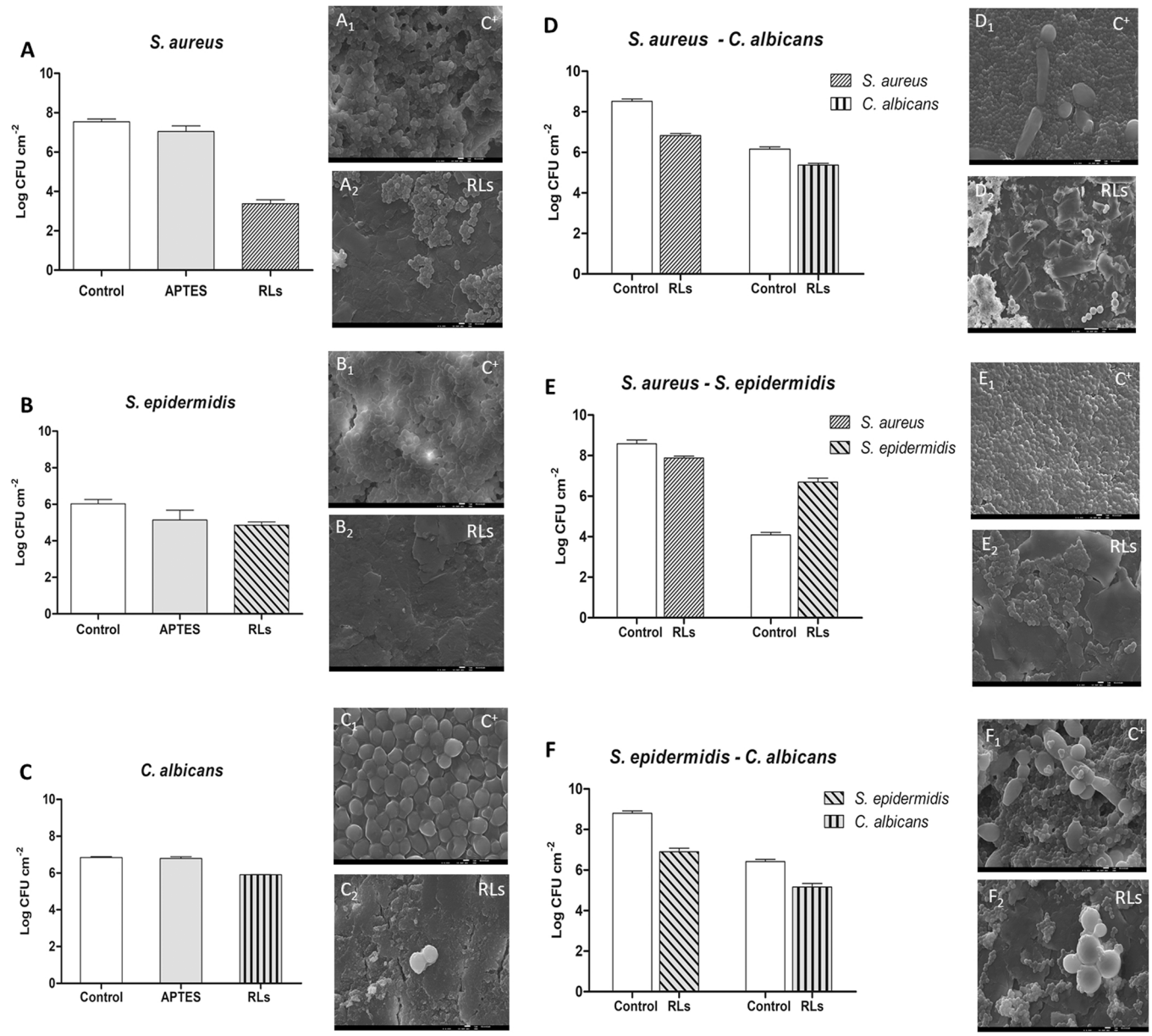

Fig. 3. Biofilm inhibition of RLs surfaces against mono-incubation of *S. aureus, S. epidermidis* and C. *albicans* **(A-C)** and against co-incubations of *S. aureus- C. albicans; S. aureus- S. epidermidis* and *S. epidermidis - C. albicans* **(D-F)**. Biofilm inhibition was assessed by colony forming unit counts **(A-F)**. Scanning electron microscopy allowed the visualization of controls ($\mathbf{A_1}$-$\mathbf{F_1}$) and functionalized samples surfaces ($\mathbf{A_2}$-$\mathbf{F_2}$) colonization; C+ stands for positive control (plain PDMS). Images magnification at 4000x.

3.2.1. *Surface characterization*

3.2.1.1. Wettability. Modifications in surface wettability were evaluated by contact angle measurements of PDMS surfaces before and after functionalization (Fig. 2A). Surface modification with RLs mixture (PDMS-RLs) offered high hydrophilicity to the PDMS surface observed with the decrease in the contact angle measurements from 95 ° (plain PDMS) to 17 ° (PDMS-RLs). This sharp decrease in the contact angle measurement confirms surface modification occurring after the functionalization reaction associated to the presence of the polar groups such as hydroxyl groups originated from surface oxidation, and RLs functionalization [27].

3.2.1.2. XPS and FTIR-ATR. Successful functionalization of PDMS surface with RLs mixture was ascertained through high-resolution XPS spectra (Fig. 2B). From the PDMS and PDMS-RLs XPS spectra the presence of carbon, oxygen, silanol peak components can be observed. After the PDMS reacted with RLs mixture, the effective anchoring of RLs was confirmed by the appearance of nitrogen, NH-C(=O)- (N1s at 400.17 eV) [40] in the N1s spectrum (Fig. 2B). The XPS spectrum of the PDMS exhibited a O1s/C1s photoemissions ratio of 1.09, while for the PDMS-RLs the ratio determined was 0.48, which indicates that the functionalization with RLs changed the PDMS surface chemical compositions by introducing more carbon. After curve-fitting, it can be observed that the high-resolution C1s XPS spectra of the PDMS exhibited four peaks, two well defined at 284.8 eV (C-Si/C-C/ C-H) and 285.5 eV (C-OH), and one small peak at 286.6 eV (C-O/C-N) [41,42]. However, in the C 1 s core-level spectrum of the PDMS-RLs surface (Fig. 1X) five peak components were detected at about 284.8, 285.6, 286.6, 288.0 and 289.2 eV, attributable to the (C-Si/C-C/ C-H), (C-OH), (C-O/C-N), C═O and (O-C═O) species, respectively [40,43,44]. The appearance of C-N, as well as C═O and O-C═O species confirmed the presence of RLs on the

PDMS surface [45]. The Si 2p spectra show that pristine organic silicone phase or PDMS backbone Si(-O)2 and surface Si(-O)1 are most prevalent on the PDMS-RLs surface. The more highly oxidized Si(-O)3 and Si(-O)4 components at higher binding energy decrease in intensity on the PDMS-RLs surface, which illustrates the different chemical environment of Si atoms after functionalization when compared to PDMS surface [46].

The chemical characteristics of PDMS surface modification with RLs mixture (PDMS-RLs) was also investigated by ATR-FTIR spectroscopy. The ATR-FTIR spectrums of PDMS and PDMS-RLs are shown in Fig. 2C. Several characteristic FT-IR peaks of PDMS are observed [47]. Similarly, in the ATR-FTIR spectrum of PDMS-RLs, the same PDMS functional groups were observed. Moreover, RLs characteristic FTIR peaks present in RLs powder [48] also appeared in PDMS-RLs. After functionalization, representative peaks of the amide functional group appeared namely, the C-N bond at 1450 cm^{-1}, the N-H bond at 1554 cm^{-1} and the C═O bond at 1650 cm^{-1} indicating successful binding of rhamnolipid to PDMS [49].

3.2.2. Protein adsorption

It was possible to observe that RLs-functionalized PDMS increased surface antifouling ability since a 36% decrease on BSA adsorption was observed when comparing to the plain PDMS (Fig. 2D). Thus, the value of the BSA concentration decreased from 0.075 ± 0.009 mg cm^{-2} on the plain PDMS, to 0.048 ± 0.005 mg cm^{-2} after RLs' functionalization and according to Faustino et al. [50], this reduction could be assigned to the increase in the surface hydrophilicity which might interrupt the hydrophobic interactions that leads to the fouling phenomenon.

3.3. Antibiofilm activity

In order to assess the antimicrobial efficiency of the RLs' functionalized PDMS, the antibiofilm activity towards mono and dual species of prevailing bacteria and fungi in the blood stream catheter related infections were evaluated. For individual species, a surprising performance of the RLs' functionalized PDMS against *S. aureus* (Fig. 3 A) was observed with a log reduction of 4.20 (99.99%). A log reduction of 1.17 and 0.95 (93.26% and 88.78%) was also observed against *S. epidermidis* and *C. albicans* respectively (Fig. 3B and C). For all the assays, comparison was with respect to the positive controls (plain PDMS). SEM images confirmed the CFUs' previous results. Thus, the multilayered colonies observed on the plain PDMS material used as positive control (Figure $3A_1$, B_1, C_1), were efficiently reduced when functionalizing the PDMS surfaces with RLs glycolipids, against all the used strains (Figure $3A_2$, B_2, C_2). Regarding APTES functionalized specimens no considerable differences from positive controls were observed. Thus, APTES samples were not tested in dual species assays.

When in dual-species culture with *C. albicans*, *S. aureus and S. epidermidis* biofilm was reduced in 1.69 and 1.9 log (CFU) (97.95% and 98.74%), respectively regarding the RLs-functionalized samples when compared to control. In the same samples *C. albicans* biofilm formation log (CFU) decreased 0.79 and 1.26 (83.78% and 94.50%) when cultured with *S. aureus* and *S. epidermidis,* respectively (Fig. 3). Ceresa et al. [28] when performing experiments using silicone discs coated (by adsorption) with RLs biosurfactants also found that surfaces were effective against dual species biofilms *(S. aureus- C. albicans* and *S. epidermidis - C. albicans)*. After 24 h they found a biofilm biomass inhibition and a metabolic activity reduction of 95.1% and 95.6%, respectively.

When comparing microorganisms' numbers on biofilm formed in mono with dual-culture assays it was possible to observe that *S. aureus* and *S. epidermidis* surface colonization was higher when in co-culture with *C. albicans.* This is in accordance with Ceresa et al.[28] who found that the biomass and the metabolic activity of the dual-species biofilms of *Staphylococcus spp.-C. albicans* were higher than those of the mono-species biofilms up to 72 h for *S. aureus* ATCC 25923, and up to 48 h for *S. epidermidis* ATCC 35984. Moreover, Peter et al. [37] stated that *C. albicans* may present a nidus or scaffolds for *S. aureus* in order to facilitate its adherence to the catheter surface and protect *staphylococcus spp* by secreting an extracellular matrix.

Regarding *S. aureus-S. epidermidis* co-culture assays a log reduction of 1.69 (97.96%) was observed for *S. aureus* biofilm in RLs-functionalized surfaces (Fig. 3). Moreover, a log reduction of 1.94 was observed when comparing *S. epidermidis* control values in single-biofilm with *S. aureus* dual-biofilm (Fig. 3 E). These results can be attributed to the competitive behavior of the mixed *staphylococcus* spp. in the binary biofilm, revealed also in this study by *S. aureus* that had a significant competitive advantage over the strain *S. epidermidis* on the positive control surfaces which could be confirmed by a log increment of 1.05 when comparing *S. aureus* single-biofilm *with S. epidermidis* dual-biofilm (Fig. 3 A). This is in accordance with Gannesen et al. [51] who found that the *S. aureus* MFP03 possessed a competitive advantage over of *S. epidermidis* MFP04 in both planktonic co-culture and binary biofilms. Two mechanisms might be behind this observation: the first suggestion is that *S. aureus* was a very strong competitor and had the advantage to adhere to the catheter surface over *S. epidermidis* and the second suggestion can be attributed to the full charge of the surface covered *S. aureus* and the absence of free sites for *S. epidermidis* to adhere [52].

In accordance with the upper findings, the SEM analysis of the dual species confirmed the presence of the different studied bacteria and fungi on surfaces of the RLs- functionalized PDMS and plain PDMS (control). High contact was observed between *S. aureus* and *C. albicans* hyphae in which *S. aureus'* cells could easily cover the *C. albicans* architecture (Figure $3D_1$). However, since *S. epidermidis* tends to adhere less to the surface less contact with *C. albicans* hyphae was observed (the architecture is more open than that with *S. aureus*) (Figure 3 F_1). This difference in interaction between bacteria and yeast hyphae might be due to the differential protein expression of the different bacteria that has been reported by Peter *et al.* [53].

Thus, the three-dimensional and multilayered microbial biofilms observed in the control substrates (Figure $3D_1$, E_1, F_1) were reduced when using the RLs-functionalized PDMS samples since the majority of the RLs-functionalized PDMS samples' surfaces exhibited small and dispersed cell clusters (Figure $3D_2$, E_2, F_2). Additionally, the hyphal yeasts' cell form existing in the PDMS positive controls (Figure $3D_1$, F_1), were reduced with the RLs-functionalized PDMS samples (Figure $3D_2$, F_2) which is considered as an interesting outcome since the presence of the hyphal yeasts' cell forms plays a crucial role in the *C. albicans* pathogenic fungal infections [54].

In RLs-functionalized samples the glycolipids might act through their antimicrobial and anti-adhesive properties since when in contact with the microbial cell walls, RLs have the ability to change the hydrophobicity of the cell surface and increase its permeability [28]. In addition, regarding the substrate surface, the RLs might limit the microbial adhesion phenomenon and by consequence the bacterial and/or fungal biofilm formation by acting on the physical-chemical properties of the PDMS surface (e.g. wettability, topography) making it unfavorable for bacteria/fungi adhesion [28]. For instance, *S. aureus* ATCC 25923 has shown in a previous work [33] a partition coefficient of 69.5% thus presenting a higher affinity for the hydrophobic phase. When functionalizing PDMS surface with RLs by oxidation and carbodiimide reaction the surface become considerably more hydrophilic (showing contact angle values of 17.26 ± 2.43) and that will lead to a lower attach of bacteria that have affinity for the hydrophobic phases.

Regarding global results RLs-PDMS surfaces seemed more effective in reducing bacteria than *C. albicans* biofilms. In the herein presented work the MIC values of the RLs mixture towards *S. aureus* and *S. epidermidis* were determined as 100 and 200 μg mL^{-1}, respectively while for *C. albicans* that value was considered higher than 800 μg mL^{-1}. Consequently, the higher antibiofilm activity of RLs-PDMS observed towards bacteria is probably aligned with the lower MIC value observed for bacteria when compared to *C. albicans.* The reduced antibiofilm effect observed in *C. albicans* is likely to be related only to the compound's

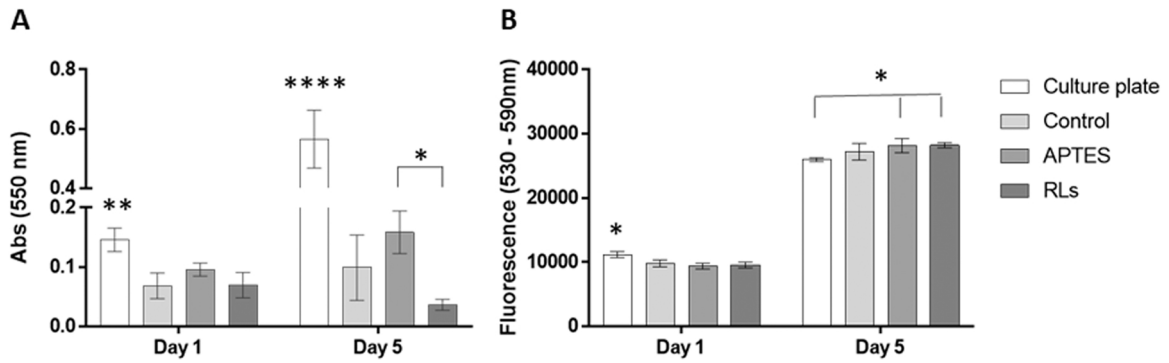

Fig. 4. **A**. Metabolic activity/Viability assay of human dermal fibroblasts cultures. MTT assay of cultures established directly on the materials' surface. **B.** Resazurin assay of cells cultured grown in the presence of materials' leachables. *p < 0.05; * *p < 0.01; * ** *p < 0.0001.

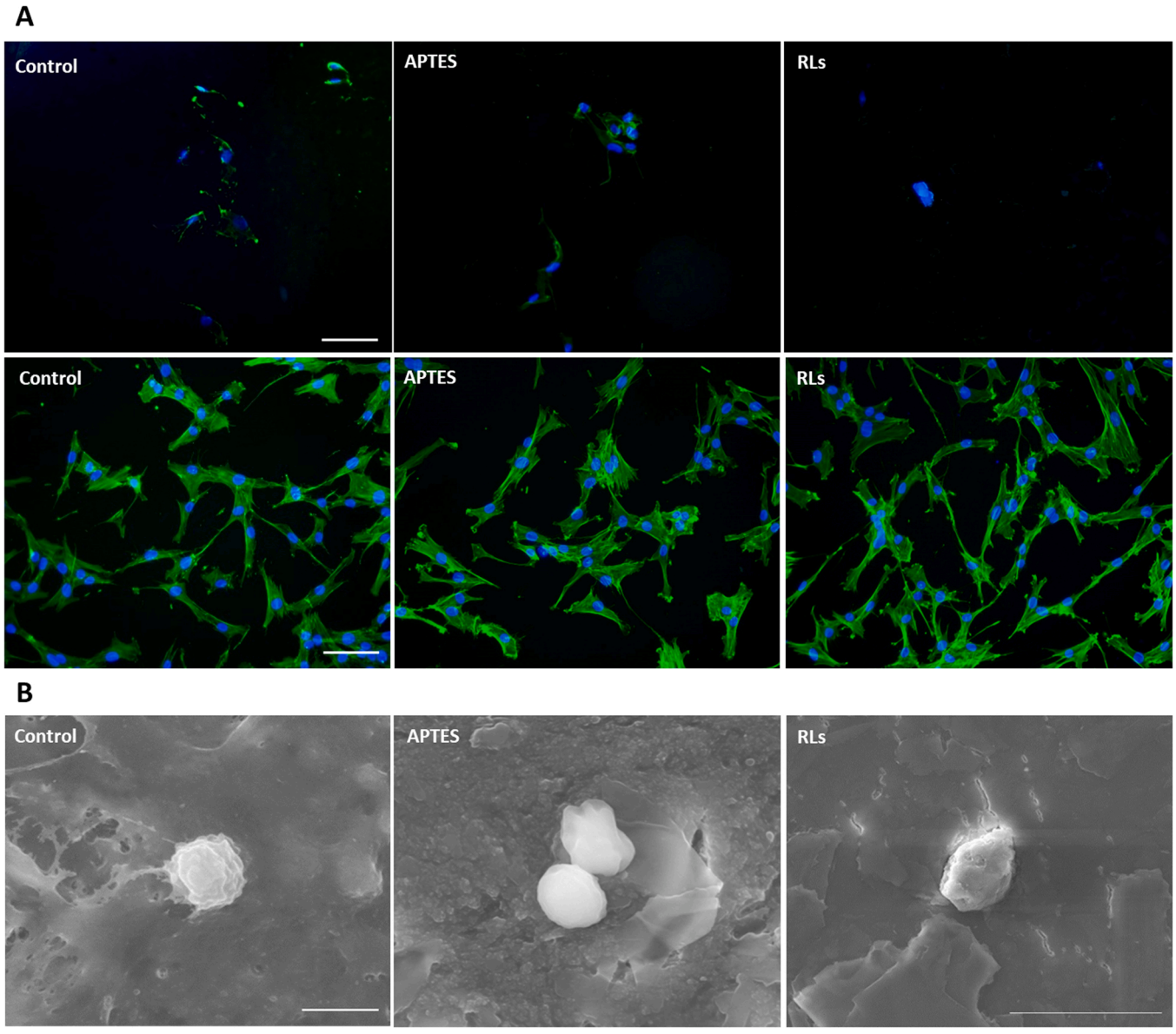

Fig. 5. A. Representative fluorescence images of human dermal fibroblasts morphology grown for 1 day. Cells were stained for actin cytoskeleton in green and counter-stained for the nucleus in blue. The upper panel corresponds to cells cultured directly on the materials' surface, while the lower panel corresponds to cells cultured in the presence of materials' leachables. Scale bar corresponds to 100 μm. B. Platelet adhesion assay. Representative SEM images of adhered platelets over the materials' surface. Scale 2 μm.

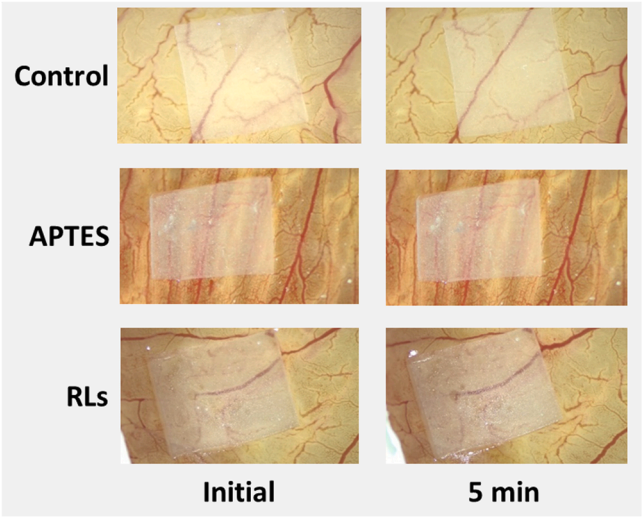

Experimental condition	Lysis	Hemorrhage	Coagulation	Total irritation score (IS)
C- (NaCl)	0	0	0	0
C+ (NaOH)	5	7	5	17
Control	0	0	0	0
APTES	0	0	0	0
RLs	0	0	0	0

Fig. 6. Representative *in ovo* images of the HET-CAM assay of the materials for the first (0.5 min) and the last (5 min) time points and quantitative irritation score.

antiadhesive effect.

3.4. Biocompatibility evaluation - In vitro cytocompatibility and hemocompatibility assessment

The cytocompatibility of the developed materials was assessed using human fibroblastic cells. Significant differences regarding cellular response were observed between cultures grown directly on the materials and those grown only in the presence of materials' leachables (Figs. 4 and 5). Cells cultured directly on materials' surface (Fig. 4 A) presented significant lower MTT reduction values when compared to those of cells cultured on the bottom of the culture plate, which were found to increase from day 1 to day 5. Comparatively, day-1 values were around 50% lower to those of culture plate values, while, at day 5, a reduction of around 80% was attained, for all experimental conditions.

On the other hand, regarding cultures grown in the presence of materials' leachables – all experimental groups presented a high metabolic activity, increasing from day 1 to day 5, in a similar manner to that of cultures grown in the absence of leachables (culture plate) (Fig. 4B). At day 1, metabolic activity of all experimental groups was found to be marginally lower in relation to culture plate while, at day 5, APTES and RLs groups presented significant higher levels in comparison to culture plate levels.

The assessment of the cell morphology and culture organization performed by fluorescence imaging, at day 1 of culture, revealed a similar trend (Fig. 5 A) – cells cultured on the tissue culture plate presented a spread and stretched morphology, well-organized actin stress fibers, with distributed cytoplasmic extensions, as well as cell-to-cell contacts and cellular philopodia (supplementary material SM2). Nevertheless, the direct assessment of the materials' surface revealed a very low number of adhered cells presenting a shrunk and irregular cytoplasm, with a disturbed organization (Fig. 5 A upper panel). In addition, the morphological organization of cells cultured in the presence of leachables – independently of the material, i.e. control, APTES or RLs – was found to be indistinguishable from those cultured in tissue culture plates, presenting similar morphological characteristics and cellular arrangement, as previously described (Fig. 5 A lower panel).

Overall, a distinctive human fibroblastic response was verified in the assayed experimental setup. An impaired cellular adhesion and reduced metabolic activity was identified on control, APTES and RLs materials within the direct assay; while a high cell adhesion, metabolic activity and proliferation - similar to those attained in the culture plate - were verified within the indirect assay, for all experimental materials. This behavior is envisioned for the given target application – vascular catheters – in which the adhesion and proliferation of cells are undesirable, given the risk of catheter occlusion and thrombus/embolus formation, while at the same time, no cytotoxic response is envisaged by leachable components into the surrounding tissues [55,56].

Hemocompatibility evaluation was based on the platelet adhesion assay, characterized by SEM imaging (Fig. 5B). Upon adhesion, platelets presented a broadly round morphology on the control surface, similar to that verified for both APTES and RLs samples. Minimal spreading and extension of pseudopia were verified, for all the assayed materials. Platelet adhesion and activation are critical indexes for evaluating blood compatibility to artificial surfaces, being recognized as early indicators of the thrombogenicity of blood contacting implants [56]. The attained morphology, evidencing a round/discoid structure with the absence of pseudopodia and hyaloplasma spreading supports a limited platelet activation, in accordance with previous data supporting the capability of PDMS to lessen platelet adhesion/activation [57], not being significantly modified by the APTES or RLS functionalization [58].

3.5. Vascular irritation assessment

The HET-CAM assay was performed to evaluate the vascular irritation potential of the materials (Fig. 6). Regarding the characterization of the developed materials, no macroscopic alterations were observed, in a similar fashion to the negative control group, indicating a non-irritating profile for the materials. Comparatively, the positive control presented significant vascular alterations, namely lysis, hemorrhage and coagulation, greatly compromising the functionality of the vascular network (SM3). As a result, no scores regarding lysis, hemorrhage nor coagulation were assigned for experimental groups and the negative control, presenting a total irritation score of 0; while the positive control scored 17, being regarded as severely irritating. In accordance with the attained data, distinct viscosity PDMS materials were previously found to present no vascular irritation potential as recently addressed within the HET-CAM assay [59], and also within in vivo applications [60].

4. Conclusions

Overall, this work showed that rhamnolipids were successfully bonded onto medical grade PDMS surface and that this functionalization improved the surface antiadhesive and antimicrobial properties. Not only the produced surfaces were active against mono-species biofilms but also towards dual-species biofilms. Moreover, the produced surfaces showed biocompatibility features regarding cytocompatibility, platelet activation and vascular irritation. Eliminating polymicrobial biofilm infections is certainly a challenge and rhamnolipids-functionalized medical grade PDMS may become an option regarding the reduction of medical devices related infections.

CRediT authorship contribution statement

Maissa Dardouri: Methodology, Validation, Formal analysis, Investigation, Writing – original draft. **Israa Aljnadi**: Investigation. **Jonas Deuermeie:** Investigation. **C. Santos:** Validation, Writing – original draft. **Victor Martin**: Investigation, Methodology. **Fabiola**

Costa: Methodology. **M. Fernandes:** Resource**. Lídia Gonçalves**: Methodology. **Ana Bettencourt:** Writing – original draf. **P. Gomes:** Conceptualization, Supervision, Writing – review & editing. **Isabel A.C Ribeiro**: Conceptualization, Validation, Resources, Writing – original draft, Writing – review & editing, Visualization, Supervision, Project administration, Funding acquisition.

Declaration of Competing Interest

The authors declare no conflicts of interest**.**

Acknowledgements

The authors thank Fundação para a Ciência e Tecnologia (FCT) Portugal, for the financial support under the Project PTDC/BTM-SAL/29335/2017. Portugal 2020 for the Portuguese Mass Spectrometry Network (Rede Nacional de Espectrometria de Massa RNEM) is also acknowledged. The authors also acknowledge the Designer Nuno Monge for the artwork, Isabel Dias Nogueira (Microlab, Instituto Superior Técnico, Lisbon University) for the technical assistance with the SEM analysis, Andreia Bento for the assistance with the UHPLC-MS equipment (iMed.Ulisboa) and Professor Maria José Ferreira (FFULisboa) for allowing the use of the automatic flash chromatography equipment.

Appendix A. Supporting information

Supplementary data associated with this article can be found in the online version at doi:10.1016/j.colsurfb.2022.112679.

References

[1] V. Prabhawathi, K. Thirunavukarasu, M. Doble, A study on the long term effect of biofilm produced by biosurfactant producing microbe on medical implant, Mater. Sci. Eng. C. 40 (2014) 212–218, https://doi.org/10.1016/j.msec.2014.03.050.
[2] N.G. Simões, A.F. Bettencourt, N. Monge, I.A.C. Ribeiro, Novel antibacterial agents: an emergent need to win the battle against infections, Mini-Rev. Med. Chem. 17 (2017) 1364–1376, https://doi.org/10.2174/1389557516666160907151454.
[3] S.-H. Wang, T.W.-H. Tang, E. Wu, D.-W. Wang, C.-F. Wang, Y.-D. Liao, Inhibition of bacterial adherence to biomaterials by coating antimicrobial peptides with anionic surfactant, Colloids Surf. B Biointerfaces 196 (2020), 111364, https://doi.org/10.1016/j.colsurfb.2020.111364.
[4] S. Jiang, C.P. Teng, Fabrication of silver nanowires-loaded polydimethylsiloxane film with antimicrobial activities and cell compatibility, Mater. Sci. Eng. C. 70 (2017) 1011–1017, https://doi.org/10.1016/j.msec.2016.04.094.
[5] Y. Sun, Y. Lang, Z. Yan, L. Wang, Z. Zhang, High-throughput sequencing analysis of marine pioneer surface-biofilm bacteria communities on different PDMS-based coatings, Colloids Surf. B Biointerfaces 185 (2020), 110538, https://doi.org/10.1016/j.colsurfb.2019.110538.
[6] A. Gokaltun, M.L. Yarmush, A. Asatekin, O.B. Usta, Recent advances in nonbiofouling PDMS surface modification strategies applicable to microfluidic technology, TECHNOLOGY 05 (2017) 1–12, https://doi.org/10.1142/S2339547817300013.
[7] T. Vila, E.F. Kong, D. Montelongo-Jauregui, P. Van Dijck, A.C. Shetty, C. McCracken, V.M. Bruno, M.A. Jabra-Rizk, Therapeutic implications of C. albicans-S. aureus mixed biofilm in a murine subcutaneous catheter model of polymicrobial infection, Virulence 12 (2021) 835–851, https://doi.org/10.1080/21505594.2021.1894834.
[8] H. Carolus, K. Van Dyck, P. Van Dijck, Candida albicans and staphylococcus species: a threatening twosome, Front. Microbiol 10 (2019), https://doi.org/10.3389/fmicb.2019.02162.
[9] W.F. Oliveira, P.M.S. Silva, R.C.S. Silva, G.M.M. Silva, G. Machado, L.C.B. B. Coelho, M.T.S. Correia, Staphylococcus aureus and Staphylococcus epidermidis infections on implants, J. Hosp. Infect. 98 (2018) 111–117, https://doi.org/10.1016/j.jhin.2017.11.008.
[10] A. Vaterrodt, B. Thallinger, K. Daumann, D. Koch, G.M. Guebitz, M. Ulbricht, Antifouling and antibacterial multifunctional polyzwitterion/enzyme coating on silicone catheter material prepared by electrostatic layer-by-layer assembly, Langmuir 32 (2016) 1347–1359, https://doi.org/10.1021/acs.langmuir.5b04303.
[11] M.R. Nejadnik, A.F. Engelsman, I.C. Saldarriaga Fernandez, H.J. Busscher, W. Norde, H.C. van der Mei, Bacterial colonization of polymer brush-coated and pristine silicone rubber implanted in infected pockets in mice, J. Antimicrob. Chemother. 62 (2008) 1323–1325, https://doi.org/10.1093/jac/dkn395.
[12] M.M. Sugii, F.A. de, S. Ferreira, K.C. Müller, D.A.N.L. Lima, F.C. Groppo, H. Imasato, U.P. Rodrigues-Filho, F.H.B. Aguiar, Physical, chemical and antimicrobial evaluation of a composite material containing quaternary ammonium salt for braces cementation, Mater. Sci. Eng. C. 73 (2017) 340–346, https://doi.org/10.1016/j.msec.2016.12.084.
[13] S. Zanini, A. Polissi, E.A. Maccagni, E.C. Dell'Orto, C. Liberatore, C. Riccardi, Development of antibacterial quaternary ammonium silane coatings on polyurethane catheters, J. Colloid Interface Sci. 451 (2015) 78–84, https://doi.org/10.1016/j.jcis.2015.04.007.
[14] J.S. VanEpps, J.G. Younger, Implantable device-related infection, Shock 46 (2016) 597–608, https://doi.org/10.1097/SHK.0000000000000692.
[15] I. Raad, R. Darouiche, R. Hachem, M. Mansouri, G.P. Bodey, The broad-spectrum activity and efficacy of catheters coated with minocycline and rifampin, J. Infect. Dis. 173 (1996) 418–424, https://doi.org/10.1093/infdis/173.2.418.
[16] A. Salvarci, M. Koroglu, T. Gurpinar, Evaluation of antimicrobial activities of minocycline and rifampin-impregnated silicone surfaces in an in vitro urinary system model, J. Pak. Med. Assoc. 65 (2015) 115–119.
[17] M. Ferreira, O. Rzhepishevska, L. Grenho, D. Malheiros, L. Gonçalves, A. J. Almeida, L. Jordão, I.A. Ribeiro, M. Ramstedt, P. Gomes, A. Bettencourt, Levofloxacin-loaded bone cement delivery system: highly effective against intracellular bacteria and Staphylococcus aureus biofilms, Int. J. Pharm. 532 (2017) 241–248, https://doi.org/10.1016/j.ijpharm.2017.08.089.
[18] T.A. Gaonkar, L.A. Sampath, S.M. Modak, Evaluation of the antimicrobial efficacy of urinary catheters impregnated with antiseptics in an in vitro urinary tract model, Infect. Control Hosp. Epidemiol. 24 (2003) 506–513, https://doi.org/10.1086/502241.
[19] M.L.W. Knetsch, L.H. Koole, New strategies in the development of antimicrobial coatings: the example of increasing usage of silver and silver nanoparticles, Polymers 3 (2011) 340–366, https://doi.org/10.3390/polym3010340.
[20] A. Siddique, I. Pause, S. Narayan, L. Kruse, R.W. Stark, Endothelialization of PDMS-based microfluidic devices under high shear stress conditions, Colloids Surf. B Biointerfaces 197 (2021), 111394, https://doi.org/10.1016/j.colsurfb.2020.111394.
[21] A. Gökaltun, Y.B. Kang, M.L. Yarmush, O.B. Usta, A. Asatekin, Simple surface modification of poly(dimethylsiloxane) via surface segregating smart polymers for biomicrofluidics, Sci. Rep. 9 (2019) 7377, https://doi.org/10.1038/s41598-019-43625-5.
[22] R. Mishra, A.K. Panda, S. De Mandal, M. Shakeel, S.S. Bisht, J. Khan, Natural anti-biofilm agents: strategies to control biofilm-forming pathogens, Front. Microbiol. 11 (2020), https://doi.org/10.3389/fmicb.2020.566325.
[23] D. Maji, S.K. Lahiri, S. Das, Study of hydrophilicity and stability of chemically modified PDMS surface using piranha and KOH solution, Surf. Interface Anal. 44 (2012) 62–69, https://doi.org/10.1002/sia.3770.
[24] R.M. Mendes, A.P. Francisco, F.A. Carvalho, M. Dardouri, B. Costa, A. F. Bettencourt, J. Costa, L. Gonçalves, F. Costa, I.A.C. Ribeiro, Fighting S. aureus catheter-related infections with sophorolipids: electing an antiadhesive strategy or a release one? Colloids Surf. B Biointerfaces 208 (2021), 112057 https://doi.org/10.1016/j.colsurfb.2021.112057.
[25] M. Dardouri, A. Bettencourt, V. Martin, F.A. Carvalho, C. Santos, N. Monge, N. C. Santos, M.H. Fernandes, P.S. Gomes, I.A.C. Ribeiro, Using plasma-mediated covalent functionalization of rhamnolipids on polydimethylsiloxane towards the antimicrobial improvement of catheter surfaces, Mater. Sci. Eng. C. (2021), 112563, https://doi.org/10.1016/j.msec.2021.112563.
[26] P. Thakur, N.K. Saini, V.K. Thakur, V.K. Gupta, R.V. Saini, A.K. Saini, Rhamnolipid the Glycolipid Biosurfactant: Emerging trends and promising strategies in the field of biotechnology and biomedicine, Microb. Cell Fact. 20 (2021) 1–15, https://doi.org/10.1186/s12934-020-01497-9.
[27] C. Ceresa, F. Tessarolo, D. Maniglio, E. Tambone, I. Carmagnola, E. Fedeli, I. Caola, G. Nollo, V. Chiono, G. Allegrone, M. Rinaldi, L. Fracchia, Medical-grade silicone coated with rhamnolipid R89 is effective against Staphylococcus spp. Biofilms, Molecules 24 (2019), https://doi.org/10.3390/molecules24213843.
[28] C. Ceresa, M. Rinaldi, F. Tessarolo, D. Maniglio, E. Fedeli, E. Tambone, P. Caciagli, I.M. Banat, M.A. Diaz De Rienzo, L. Fracchia, Inhibitory effects of lipopeptides and glycolipids on C. albicans–Staphylococcus spp. dual-species biofilms, Front. Microbiol 11 (2021) 1–19, https://doi.org/10.3389/fmicb.2020.545654.
[29] M. Dardouri, R.M. Mendes, J. Frenzel, J. Costa, I.A.C. Ribeiro, Seeking faster, alternative methods for glycolipid biosurfactant characterization and purification, Anal. Bioanal. Chem. 413 (2021) 4311–4320, https://doi.org/10.1007/s00216-021-03387-4.
[30] S. Noel, B. Liberelle, L. Robitaille, G. De Crescenzo, Quantification of primary amine groups available for subsequent biofunctionalization of polymer surfaces, Bioconj. Chem. 22 (2011) 1690–1699, https://doi.org/10.1021/bc200259c.
[31] S. Armyanov, N.E. Stankova, P.A. Atanasov, E. Valova, K. Kolev, J. Georgieva, O. Steenhaut, K. Baert, A. Hubin, XPS and μ-Raman study of nanosecond-laser processing of poly(dimethylsiloxane) (PDMS), Nucl. Instruments Methods Phys. Res. Sect. B Beam Interact. with Mater. Atoms 360 (2015) 30–35, https://doi.org/10.1016/j.nimb.2015.07.134.
[32] Bio-Rad, Laboratories, Bio-Rad protein assay (Bradford), Bio Rad. (2010) 1–24.
[33] C. Pontes, M. Alves, C. Santos, M.H. Ribeiro, L. Gonçalves, A.F. Bettencourt, I.A. C. Ribeiro, Can Sophorolipids prevent biofilm formation on silicone catheter tubes? Int. J. Pharm. 513 (2016) 697–708, https://doi.org/10.1016/j.ijpharm.2016.09.074.
[34] Clinical Laboratory Standards Institute (CLSI), Reference Method for Broth Dilution Antifungal Susceptibility Testing of Yeasts., 4th ed, Wayne, PA, USA, 2017.
[35] A.C. Matos, I.A.C. Ribeiro, R.C. Guedes, R. Pinto, M.A. Vaz, L.M. Gonçalves, A. J. Almeida, A.F. Bettencourt, Key-properties outlook of a levofloxacin-loaded acrylic bone cement with improved antibiotic delivery, Int. J. Pharm. 485 (2015) 317–328, https://doi.org/10.1016/j.ijpharm.2015.03.035.
[36] T.K. Swetha, G.A. Subramenium, T. Kasthuri, R. Sharumathi, S.K. Pandian, 5-hydroxymethyl-2-furaldehyde impairs Candida albicans - Staphylococcus

epidermidis interaction in co-culture by suppressing crucial supportive virulence traits, Microb. Pathog. 158 (2021), 104990, https://doi.org/10.1016/j.micpath.2021.104990.
[37] B.M. Peters, R.M. Ward, H.S. Rane, S.A. Lee, M.C. Noverr, Efficacy of ethanol against candida albicans and staphylococcus aureus polymicrobial biofilms, Antimicrob. Agents Chemother. 57 (2013) 74–82, https://doi.org/10.1128/AAC.01599-12.
[38] V. Martin, I.A.C. Ribeiro, M.M. Alves, L. Gonçalves, A.J. Almeida, L. Grenho, M. H. Fernandes, C.F. Santos, P.S. Gomes, A.F. Bettencourt, Understanding intracellular trafficking and anti-inflammatory effects of minocycline chitosan-nanoparticles in human gingival fibroblasts for periodontal disease treatment, Int. J. Pharm. 572 (2019), 118821, https://doi.org/10.1016/j.ijpharm.2019.118821.
[39] A. Chebbi, M. Elshikh, F. Haque, S. Ahmed, S. Dobbin, R. Marchant, S. Sayadi, M. Chamkha, I.M. Banat, Rhamnolipids from Pseudomonas aeruginosa strain W10; as antibiofilm/antibiofouling products for metal protection, J. Basic Microbiol. 57 (2017) 364–375, https://doi.org/10.1002/jobm.201600658.
[40] J. Ederer, P. Janoš, P. Ecorchard, J. Tolasz, V. Štengl, H. Beneš, M. Perchacz, O. Pop-Georgievski, Determination of amino groups on functionalized graphene oxide for polyurethane nanomaterials: XPS quantitation vs. functional speciation, RSC Adv. 7 (2017) 12464–12473, https://doi.org/10.1039/C6RA28745J.
[41] T. Egghe, R. Ghobeira, P.S. Esbah Tabaei, R. Morent, R. Hoogenboom, N. De Geyter, Silanization of plasma-activated hexamethyldisiloxane-based plasma polymers for substrate-independent deposition of coatings with controlled surface chemistry, ACS Appl. Mater. Interfaces 14 (2022) 4620–4636, https://doi.org/10.1021/acsami.1c18223.
[42] K. Malecha, I. Gancarz, W. Tylus, Argon plasma-assisted PDMS–LTCC bonding technique for microsystem applications, J. Micromech. Microeng. 20 (2010), 115006, https://doi.org/10.1088/0960-1317/20/11/115006.
[43] S. Pinto, P. Alves, C.M. Matos, A.C. Santos, L.R. Rodrigues, J.A. Teixeira, M.H. Gil, Poly(dimethyl siloxane) surface modification by low pressure plasma to improve its characteristics towards biomedical applications, Colloids Surf. B Biointerfaces 81 (2010) 20–26, https://doi.org/10.1016/j.colsurfb.2010.06.014.
[44] Z. Wu, H. Zhong, X. Yuan, H. Wang, L. Wang, X. Chen, G. Zeng, Y. Wu, Adsorptive removal of methylene blue by rhamnolipid-functionalized graphene oxide from wastewater, Water Res 67 (2014) 330–344, https://doi.org/10.1016/j.watres.2014.09.026.
[45] Y. Li, H.-Y. Bi, Y.-Q. Liang, X.-M. Mao, H. Li, Synthesis of novel magnetic rhamnolipid-activated layered double hydroxides nanocomposite for simultaneous adsorption of Cu(II) and m-cresol from aqueous solution, Powder Technol. 386 (2021) 350–360, https://doi.org/10.1016/j.powtec.2021.03.048.
[46] M.R. Alexander, R.D. Short, F.R. Jones, W. Michaeli, C.J. Blomfield, A study of HMDSO/O2 plasma deposits using a high-sensitivity and -energy resolution XPS instrument: curve fitting of the Si 2p core level, Appl. Surf. Sci. 137 (1999) 179–183, https://doi.org/10.1016/S0169-4332(98)00479-6.
[47] M. Garg, Priyanka M. Chatterjee, Isolation, characterization and antibacterial effect of biosurfactant from Candida parapsilosis, Biotechnol. Rep. 18 (2018), e00251, https://doi.org/10.1016/j.btre.2018.e00251.
[48] A.F. Bettencourt, C. Tomé, T. Oliveira, V. Martin, C. Santos, L. Gonçalves, M. H. Fernandes, P.S. Gomes, I.A.C. Ribeiro, Exploring the potential of chitosan-based particles as delivery-carriers for promising antimicrobial glycolipid biosurfactants, Carbohydr. Polym. 254 (2020), 117433, https://doi.org/10.1016/j.carbpol.2020.117433.
[49] D.L.B. Robert M. Silverstein, Francis X. Webster, David J. Kiemle, Spectrometric Identification of Organic Compounds, 5th ed, ch, John Wiley and Sons, Inc, 1991.
[50] C.M.C. Faustino, S.M.C. Lemos, N. Monge, I.A.C. Ribeiro, A scope at antifouling strategies to prevent catheter-associated infections, Adv. Colloid Interface Sci. 284 (2020), 102230, https://doi.org/10.1016/j.cis.2020.102230.
[51] A.V. Gannesen, O. Lesouhaitier, A.I. Netrusov, V.K. Plakunov, M.G.J. Feuilloley, Regulation of formation of monospecies and binary biofilms by human skin microbiota components, staphylococcus epidermidis and staphylococcus aureus, by human natriuretic peptides, Microbiology 87 (2018) 597–609, https://doi.org/10.1134/S0026261718050090.
[52] M. Pihl, J.R. Davies, L.E. Chávez de Paz, G. Svensäter, Differential effects of Pseudomonas aeruginosa on biofilm formation by different strains of Staphylococcus epidermidis, FEMS Immunol. Med. Microbiol. 59 (2010) 439–446, https://doi.org/10.1111/j.1574-695X.2010.00697.x.
[53] B.M. Peters, M.A. Jabra-Rizk, M.A. Scheper, J.G. Leid, J.W. Costerton, M. E. Shirtliff, Microbial interactions and differential protein expression in Staphylococcus aureus–Candida albicans dual-species biofilms, FEMS Immunol. Med. Microbiol. 59 (2010) 493–503, https://doi.org/10.1111/j.1574-695X.2010.00710.x.
[54] J.-H. Lee, Y.-G. Kim, S.K. Khadke, A. Yamano, A. Watanabe, J. Lee, Inhibition of biofilm formation by candida albicans and polymicrobial microorganisms by nepodin via hyphal-growth suppression, ACS Infect. Dis. 5 (2019) 1177–1187, https://doi.org/10.1021/acsinfecdis.9b00033.
[55] A. Dwyer, Reducing tunneled hemodialysis catheter morbidity: surface-treated catheters-a review, Semin. Dial. 21 (2008) 542–546, https://doi.org/10.1111/j.1525-139X.2008.00499.x.
[56] I.H. Jaffer, J.C. Fredenburgh, J. Hirsh, J.I. Weitz, Medical device-induced thrombosis: what causes it and how can we prevent it? J. Thromb. Haemost. 13 (2015) S72–S81, https://doi.org/10.1111/jth.12961.
[57] D. Spiller, P. Losi, E. Briganti, S. Sbrana, S. Kull, I. Martinelli, G. Soldani, PDMS content affects in vitro hemocompatibility of synthetic vascular grafts, J. Mater. Sci. Mater. Med. 18 (2007) 1097–1104, https://doi.org/10.1007/s10856-006-0067-0.
[58] J. Li, F. Liu, X. Yu, Z. Wu, Y. Wang, Z. Xiong, J. He, APTES assisted surface heparinization of polylactide porous membranes for improved hemocompatibility, RSC Adv. 6 (2016) 42684–42692, https://doi.org/10.1039/C6RA04525A.
[59] D.G. Auliya, S. Setiadji, F. Fitrilawati, R. Risdiana, Physical characterization and in vitro toxicity test of PDMS synthesized from low-grade d4 monomer as a vitreous substitute in the human eyes, J. Funct. Biomater. 13 (2022), https://doi.org/10.3390/jfb13010003.
[60] J. Mackiewicz, B. Mühling, W. Hiebl, H. Meinert, K. Maaijwee, N. Kociok, C. Luke, Z. Zagorski, B. Kirchhof, A.M. Joussen, In vivo retinal tolerance of various heavy silicone oils, Investig. Opthalmol. Vis. Sci. 48 (2007) 1873, https://doi.org/10.1167/iovs.06-0941.